AD-A078 511 RUTGERS - THE STATE UNIV PISCATAWAY NJ DEPT OF MECHA--ETC F/G 11/6
X-RAY ANALYSIS OF ACCRUED DAMAGE IN STRESS CORROSION AND CORROS--ETC(U)
DEC 79 S WEISSMANN , R YAZICI , T TAKEMOTO N00014-77-C-0191
ONR-R-2

UNCLASSIFIED NL

1 OF 1
AD-
A 078511

END
DATE
FILMED
1-80
DDC

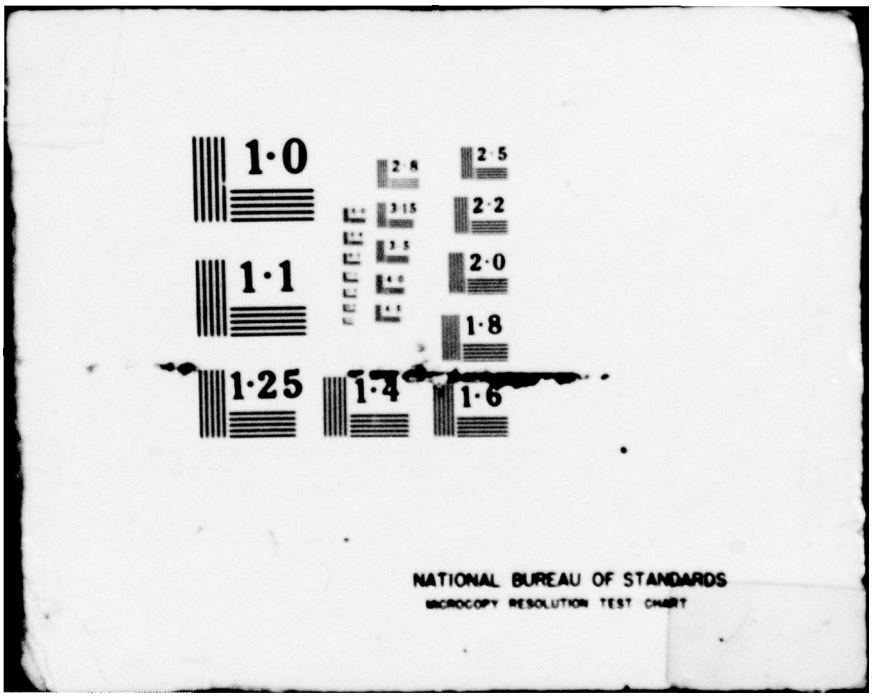
1·0
1·1
1·25
1·4
1·6
2·8
3·15
3·5
2·5
2·2
2·0
1·8
NATIONAL BUREAU OF STANDARDS
MICROCOPY RESOLUTION TEST CHART

SECURITY CLASSIFICATION OF THIS PAGE (When Data Entered)

# REPORT DOCUMENTATION PAGE

READ INSTRUCTIONS BEFORE COMPLETING FORM

| | |
|---|---|
| 1. REPORT NUMBER: ONR-R-2 | 2. GOVT ACCESSION NO. |
| 3. RECIPIENT'S CATALOG NUMBER | |
| 4. TITLE (and Subtitle): X-Ray Analysis of Accrued Damage in Stress Corrosion and Corrosion Fatigue | 5. TYPE OF REPORT & PERIOD COVERED: Interim Technical Report 1 Dec. 1978-30 Nov. 1979 |
| 6. PERFORMING ORG. REPORT NUMBER | |
| 7. AUTHOR(s): S. Weissmann, R. Yazici, T. Takemoto, T. Tsakalakos, Rutgers University, and I. R. Kramer, David W. Taylor, Naval Ship R & D Center, Annapolis, Md. | 8. CONTRACT OR GRANT NUMBER(s): N00014-77-C-0191 |
| 9. PERFORMING ORGANIZATION NAME AND ADDRESS: Department of Mechanics and Materials Science, College of Engineering, Rutgers University, Piscataway, N. J. 08854 | 10. PROGRAM ELEMENT, PROJECT, TASK AREA & WORK UNIT NUMBERS: NR 036-119 |
| 11. CONTROLLING OFFICE NAME AND ADDRESS: Office of Naval Research (Code 471) Arlington, Va. 22217 | 12. REPORT DATE: December 1, 1979 |
| | 13. NUMBER OF PAGES: 28 |
| 14. MONITORING AGENCY NAME & ADDRESS (if different from Controlling Office) | 15. SECURITY CLASS. (of this report): Unclassified |
| | 15a. DECLASSIFICATION/DOWNGRADING SCHEDULE |

LEVEL II

16. DISTRIBUTION STATEMENT (of this Report)
Approved for public release; distribution unlimited

17. DISTRIBUTION STATEMENT (of the abstract entered in Block 20, if different from Report)

DDC RECEIVED DEC 18 1979 E

18. SUPPLEMENTARY NOTES

19. KEY WORDS (Continue on reverse side if necessary and identify by block number)

| | | |
|---|---|---|
| Stress corrosion | Al 2024 | Position-sensitive detectors |
| Corrosion fatigue | X-Ray rocking curves | |
| Fracture | X-Ray topography | |
| 304 austenitic stainless steel | Fourier line profile analysis | |

20. ABSTRACT (Continue on reverse side if necessary and identify by block number)

The defect structure induced in 304 austenitic stainless steel by stress corrosion and in Al 2024 by corrosion fatigue was studied by X-ray rocking curve measurements of the grains and by X-ray Fourier analysis of the line profiles. The surface layer and bulk of the specimens were investigated, and a critical line width parameter corresponding to a critical excess dislocation density was determined that controlled the integrity of the microstructure. Improvements in the speed and efficiency of data collection were made by instrument automation and application of position-sensitive detectors.

DD FORM 1 JAN 73 1473 EDITION OF 1 NOV 65 IS OBSOLETE S/N 0102-LF-014-6601

Unclassified

SECURITY CLASSIFICATION OF THIS PAGE (When Data Entered)

79 12 18 45

(18) (19)
Report ONR-R-2

(6) X-RAY ANALYSIS OF ACCRUED DAMAGE IN STRESS CORROSION AND CORROSION FATIGUE.

(10) S. Weissmann, R. Yazici, T. Takemoto, [redacted] T. Tsakalakos
College of Engineering
Rutgers Engineering
P. O. Box 909
Piscataway, N. J. 08854

and

I. R. Kramer
David W. Taylor
Naval Ship R & D Center
Annapolis, Md.

(11) 1 Dec[redacted]1979

(9) Interim technical rept.

Report for Period 1 Dec[redacted]1978-30 Nov[redacted]1979,

(12) 30

Approved for public release; distribution unlimited

Prepared for
Office of Naval Research (Code 471)
Arlington, VA 22217

Under Contract N00014-77-C-0191

(15)



410 971

mt

TABLE OF CONTENTS


| | Page |
|---|---|
| INTRODUCTION | 3 |
| EXPERIMENTAL PROCEDURE | 4 |
| Specimen Preparation, Corrosion Media and Testing | 4 |
| RESULTS | 5 |
| Defect Structure in Surface Layer and Bulk Induced by Stress Corrosion, Fatigue and Corrosion Fatigue | 5 |
| Accrued Damage and Crack Propagation in Stress Corrosion | 8 |
| Identification and Topography of Grains Analyzed for Their Defect Structure and Stress Corrosion Specificity | 13 |
| ADVANCES IN DATA COLLECTION BY AUTOMATION AND POSITION-SENSITIVE DETECTORS | 16 |
| CONCLUSIONS | 22 |
| REFERENCES | 24 |


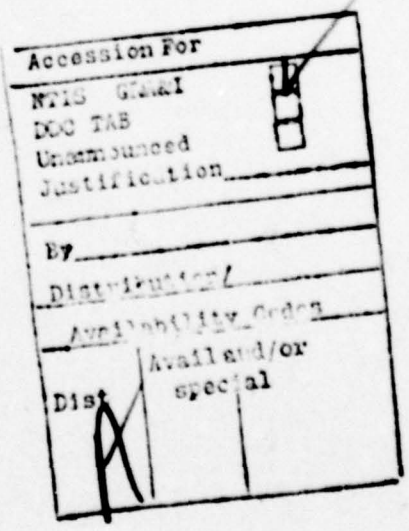

## INTRODUCTION

The X-ray studies reported in the last Interim Technical Report[1] assessed quantitatively lattice defects induced by stress corrosion (SC) in 304 stainless steel. These studies were continued, and the scope of the investigations was also extended to include studies of corrosion fatigue (CF) of 2024 aluminum alloys.

Based on the results of the previous SC studies and motivated also by the results of parallel fatigue studies of aluminum alloys,[2-4] it appears that there exists a critical excess dislocation density, $\rho^*$, above which structural failure sets in. This critical value can be assessed from measurements of the buildup of the excess dislocation densities in the surface layer and bulk of the material. It was shown that such measurements can be effectively obtained if X-ray rocking curve measurements of the grain population have been carried out. From the $\beta$ half-width of the rocking curve values, measured for various grain reflections, a statistical parameter $\bar{\beta}$ was derived that was representative of the entire grain population for the particular stage of deformation to which the specimen was subjected. The results of the studies suggest that there exists a critical half-width value, $\bar{\beta}^*$, which corresponds to the critical excess dislocation density $\rho^*$. Therefore, $\bar{\beta}^*$ may be viewed as a critical parameter that characterizes the limit of integrity of the microstructure. Consequently, if $\bar{\beta}^*$ can be predicted from $\bar{\beta}$ measurements, the remaining life of the specimen can be forecast on the basis of the nondestructive X-ray measurements.

It was shown that in order to assess $\bar{\beta}^*$ unequivocally, the buildup of excess dislocation densities must be probed in the bulk of the material; that is, in specimen regions lying beyond the quickly hardened surface layer.[1-4] Therefore, the current studies focused on the attainment of $\bar{\beta}^*$ in SC and CF studies, and on improvement and automation of experimental techniques so that $\bar{\beta}$ measurements can be performed with speed, viable for ultimate technological application. In addition, a special effort was made to elucidate the surface topography of the analyzed grains by X-ray

topography, so as to establish a bridge between the X-ray measurements and optical and electron microscopy studies of the grains by TEM and SEM.

## EXPERIMENTAL PROCEDURE

### Specimen Preparation, Corrosion Media and Testing

The austenitic stainless steel was 304 commercial grade with composition Fe-18Cr-8Ni-2Mn-1Si-0.8C. All alloys were received in sheet form, and pin-loading tensile specimens were cut with the long axis parallel to the rolling direction. The selected specimen dimensions adhered to the ASTM recommendations (ASTM Standards, Part 31, A-370), with gage dimensions 1.1" x 0.05" x 0.25". Each specimen was heat-treated prior to SC testing, to stress-relieve the specimens and to obtain a uniform grain size of 20-100 μm diameter suitable for the subsequent X-ray diffraction analysis. Specimens were placed in evacuated quartz ampoules to prevent oxidation. The specimens were heat-treated at 1100°C for 0.5 hour followed by water quench. Subsequently, the specimens were electrolytically polished. To prevent oxidation and contamination effects, a surface of at least 100 μm was removed. Care was taken to obtain flat surfaces to satisfy subsequent testing and characterization procedures. Electropolishing was also applied for the in-depth analysis of deformation induced by SC and CF. The co sive medium for austenitic stainless steel was boiling $MgCl_2$-$H_2O$ solution at 154°C.[1] The corrosive medium for the 2024-T4 alloy tested in tension-tension was a 3.5% NaCl solution. The SC tests were carried out at constant tensile load using the testing machines and testing procedures previously reported.[1]

For CF, an apparatus was constructed with a container for the corrosive medium which was made out of noncorrosive plastic. Special grips were made of MC nylon and the pins were made of stainless steel, covered with polyimide, to avoid any generation of current between grips and specimen during testing.

## RESULTS

### Defect Structure in Surface Layer and Bulk Induced by Stress Corrosion, Fatigue and Corrosion Fatigue

A tension-tension fatigue experiment of Al 2014-T4 was carried out as control experiment in a CF study. Rocking curves of the grain population were obtained, and the ratio of the average half-width over the intrinsic half-width, $\overline{\beta}/\overline{\beta}_o$, was studied as a function of depth distance from the surface for various fractions of the life. This dependence is shown in Figure 1. An analogous experiment was performed for 304 stainless steel, subjected to SC when rocking curve measurements were carried out as a function of depth distance from the surface for various fractions of corrosion time. This dependence is shown in Figure 2. Here, the dependence on corrosion time is expressed in terms of the ratio $t/t_c$, where $t_c$ signifies the critical time associated with the macroscopic mechanical instability of the structure.

Inspection of Figures 1 and 2 reveals some remarkable features that are common to both stress corrosion and metal fatigue. It will be noted that in both cases the surface layer exhibits much larger $\overline{\beta}/\overline{\beta}_o$ values than the bulk, and hence the density of excess dislocations at the surface is much greater than that of the bulk. Moreover, with increased cycling or corrosion time, the excess dislocation density in the surface layer quickly approaches saturation, while the buildup in the bulk takes place much more gradually. In both cases there exists a gradient of excess dislocation density from surface to bulk that is much steeper in the case of SC. However, in metal fatigue there exists a characteristic minimum in the gradient that has also been observed in tension-compression fatigue[2-4] and which is entirely absent in SC. This minimum is associated with a dynamical recovery effect.

The tendency for saturation of the excess dislocation density in the surface layer was also evident in CF. Figure 3 shows the dependence of $\overline{\beta}/\overline{\beta}_o$ as a function of fatigue life. The data were obtained from measurements with Cu $K_{\alpha_1}$ radiation which, due to its limiting penetration power, probed essentially the defect structure induced in the surface layer.

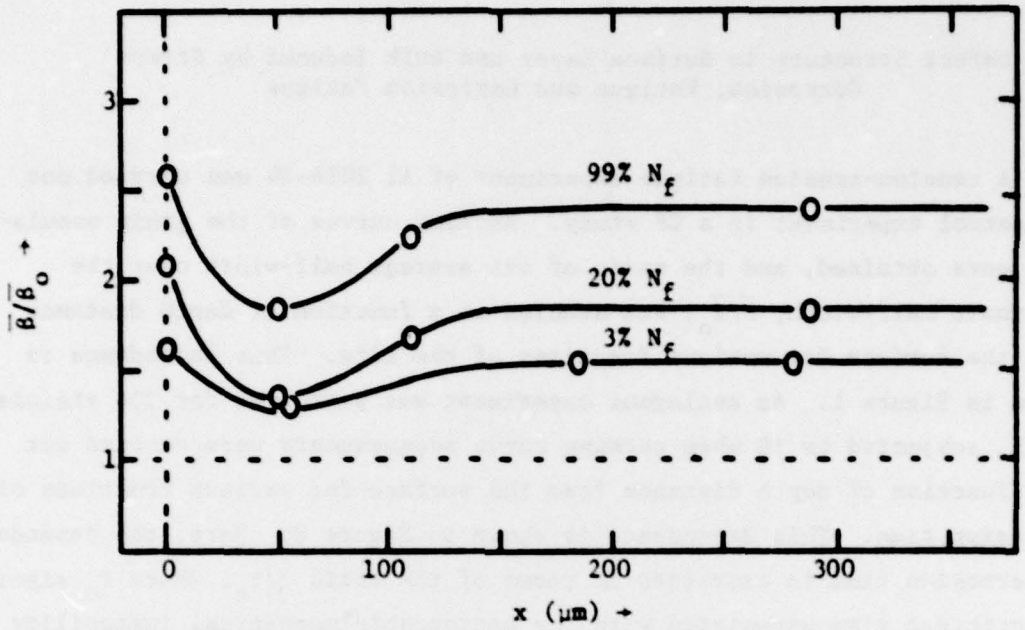


Figure 1. Dependence of $\bar{\beta}/\bar{\beta}_o$ on depth distance from surface, x (μm). Al 2014-T4 (tension-tension cycles, R = 0.2).

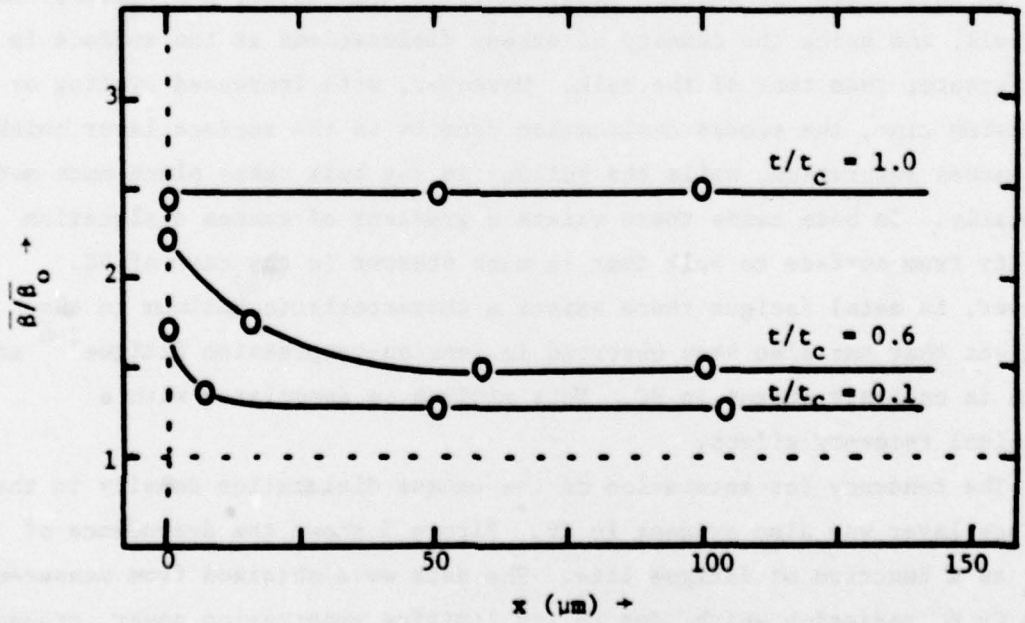


Figure 2. Dependence of $\bar{\beta}/\bar{\beta}_o$ on depth distance from surface, x (μm), for various stages of SC of 304 stainless steel.

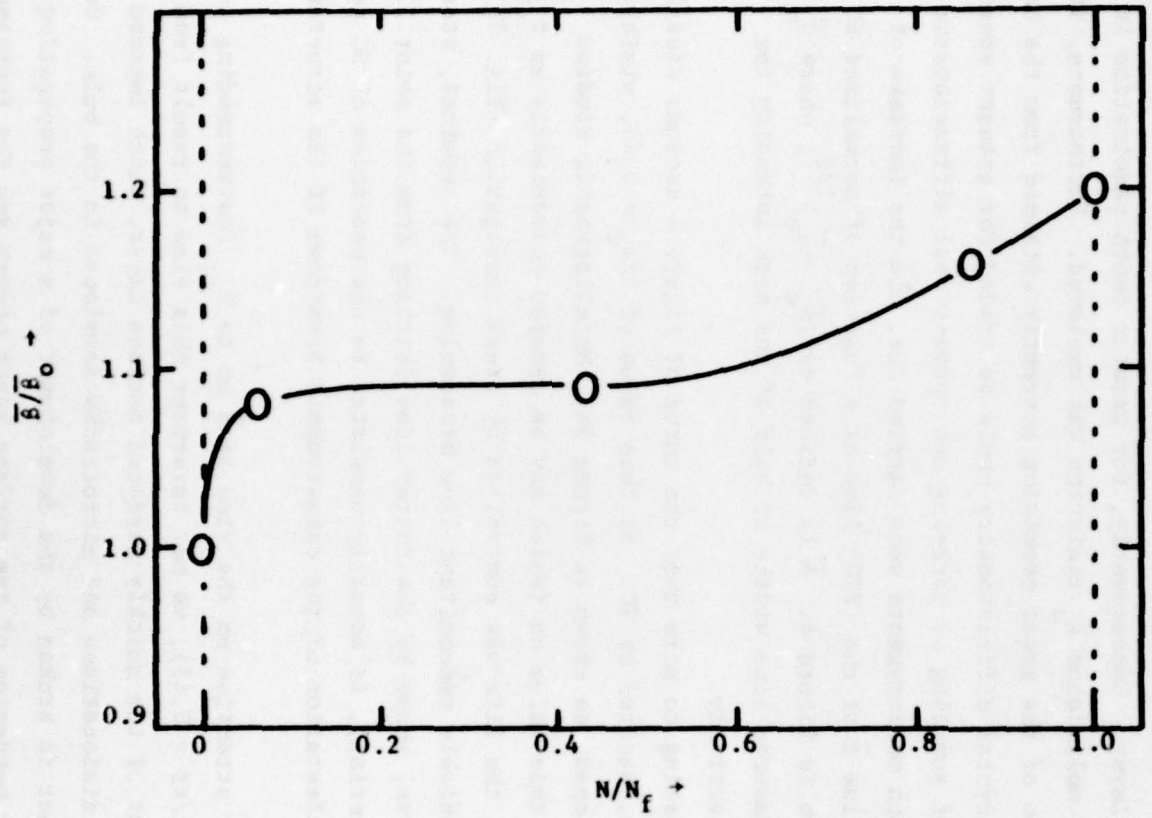


Figure 3. Dependence of $\bar{\beta}/\bar{\beta}_o$ on $N/N_f$ of Al 2024-T4 (short transverse) corrosion-fatigued at 19,000 psi - 1,900 psi in 3.5% NaCl solution (Cu $K_{\alpha_1}$ radiation).

## Accrued Damage and Crack Propagation in SC

It is apparent from Figures 1 and 2 that in order to assess the accrued damage in the material, it would be desirable to apply an X-ray beam that would be capable of penetrating at least partially beyond the quickly work-hardened surface layer. Consequently, for greater depth penetration in the measurements, molybdenum $K_\alpha$ radiation was employed. Furthermore, it was felt that some of the great precision currently attained from the use of X-ray double-crystal diffractometry could be traded for greater speed and wider range of sampling by carrying out conventional diffractometer measurements. Such measurements were carried out, and the increase of the half-width value $\bar{\beta}$ of the (220) line as a function of normalized SC time $t/t_f$ is shown in Figure 4. $\bar{\beta}$ is defined by $(\bar{\beta}_m^2 - \bar{\beta}_o)^{1/2}$, where $\bar{\beta}_m$ and $\bar{\beta}_o$ are the measured line widths at half of the peak intensity for $t/t_f$ and $t_o$, respectively.

It is interesting to note that the curve of Figure 4 ascends steeply up to the $\bar{\beta}$ value, denoted by VC. At this value of $t/t_f = 0.45$, visible cracks have developed, as shown in Figure 5a. Metallographic studies showed that from this value on (which may be denoted conveniently as $t_{cr}$), up to $t/t_f = 1.0$, the life was controlled by crack propagation (Fig. 5b) without any appreciable concomitant line broadening. The terminal, steep ascent of t. curve, shown by the dotted line starting from the point IT (initiation of tearing), is actually unrelated to the mechanism of SC per se. It is a manifestation of the catastrophic breakdown of the structure due to tearing.

Focusing our attention on the rise of $\bar{\beta}$ up to $t_{cr}$ (corresponding to $\bar{\beta} = 4.93$, $t_{cr} = t/tf = 0.45$), we may interpret this rise to result from the barrier effect of the quickly hardened surface layer, which impeded the egression of dislocations and microcracks developed in the bulk. Once this barrier effect is broken by the development of a major propagating crack, no further hardening of the surface layer occurs and the increase of line broadening virtually stops. Consequently, the $\bar{\beta}$ value corresponding to VC represents a critical value, $\bar{\beta}^*$, and the corresponding lifetime, therefore, is also denoted as $t_{cr}$.

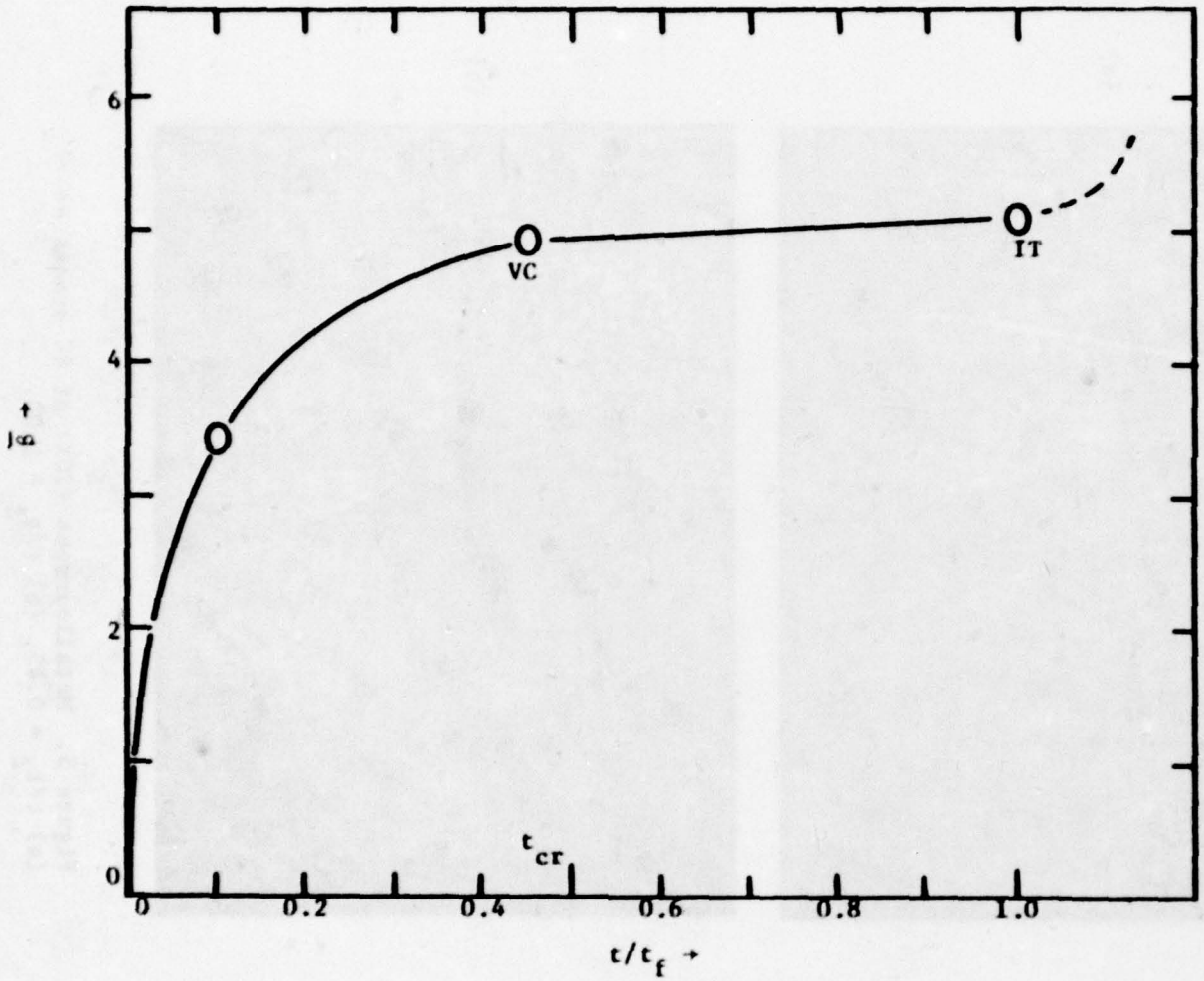


Figure 4. Dependence of line broadening on SC life (σ = 75% YS).

(a)

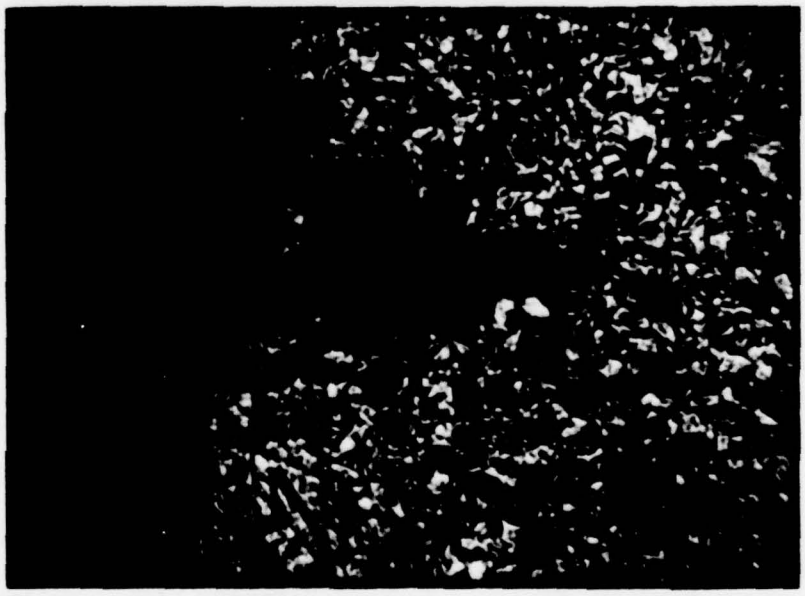

(b)

Figure 5. Metallographs (20X) of SC cracks at (a) $t/t_f = 0.45$, (b) $t/t_f = 1.00$.

Perhaps one of the most cogent reasons why the line broadening study by the conventional diffractometer method was undertaken was the fact that the results obtained by the rocking curve measurements of the grains could be checked by an independent X-ray method, namely the Warren-Averbach Fourier analysis of the life profiles.[5]

The rocking curve studies have shown that the surface layer has a special propensity over the bulk material for work hardening (Figs. 1 and 2). Through the aid of X-ray topography, it was shown that this work hardening is characterized by a breakup of the lattice into small, misaligned domains, and that these domains are separated from each other by regions in which the dislocation density is considerably larger than in the interior of these domains. The misalignment of domains is brought about by excess dislocations of one sign, and since rocking curves measure lattice misalignment, they can measure density of excess dislocations.

The Fourier analysis of the line profiles can lead to similar information. One obtains the average size of the coherently reflecting domains (particle size) $\overline{D}$, and also information about the root-mean-square lattice strain $\langle \varepsilon^2_{(L)} \rangle^{1/2}$. Of particular interest in this comparative study was the question to be answered: What is the relative contribution of particle size and lattice strain to the line broadening effect in SC?

The line profiles of the (220) and (440) reflections of a specimen subjected to SC for $t/t_f = 0.1$ were used as input data for the Fourier analysis. Referring to Figure 4, this analysis pertains to the steep ascent for the curve $\overline{B}$ vs $t/t_f$. Because the $K_\alpha$ doublet of the lines was not well separated, first the Rachinger correction for the doublet separation was performed.[6] A plot of the corrected Fourier coefficients vs the column length, L, in a given crystallographic direction is shown in Figure 6a. The extrapolation of the linear part of the plot gave an average particle size, $\overline{D} = 410$ A. The plot of $\langle \varepsilon^2_{(L)} \rangle^{1/2}$ vs L is shown in Figure 6b. It will be noted that the maximum value of $\langle \varepsilon^2_{(L)} \rangle^{1/2}$ was only $5.2 \times 10^{-4}$.

In view of the small strain value obtained, it is evident that the greatest contribution to the line broadening effect in SC derived from the fragmentation into small particles. These results, therefore, support the findings based on the measurements of the rocking curves. Cohen[7] has

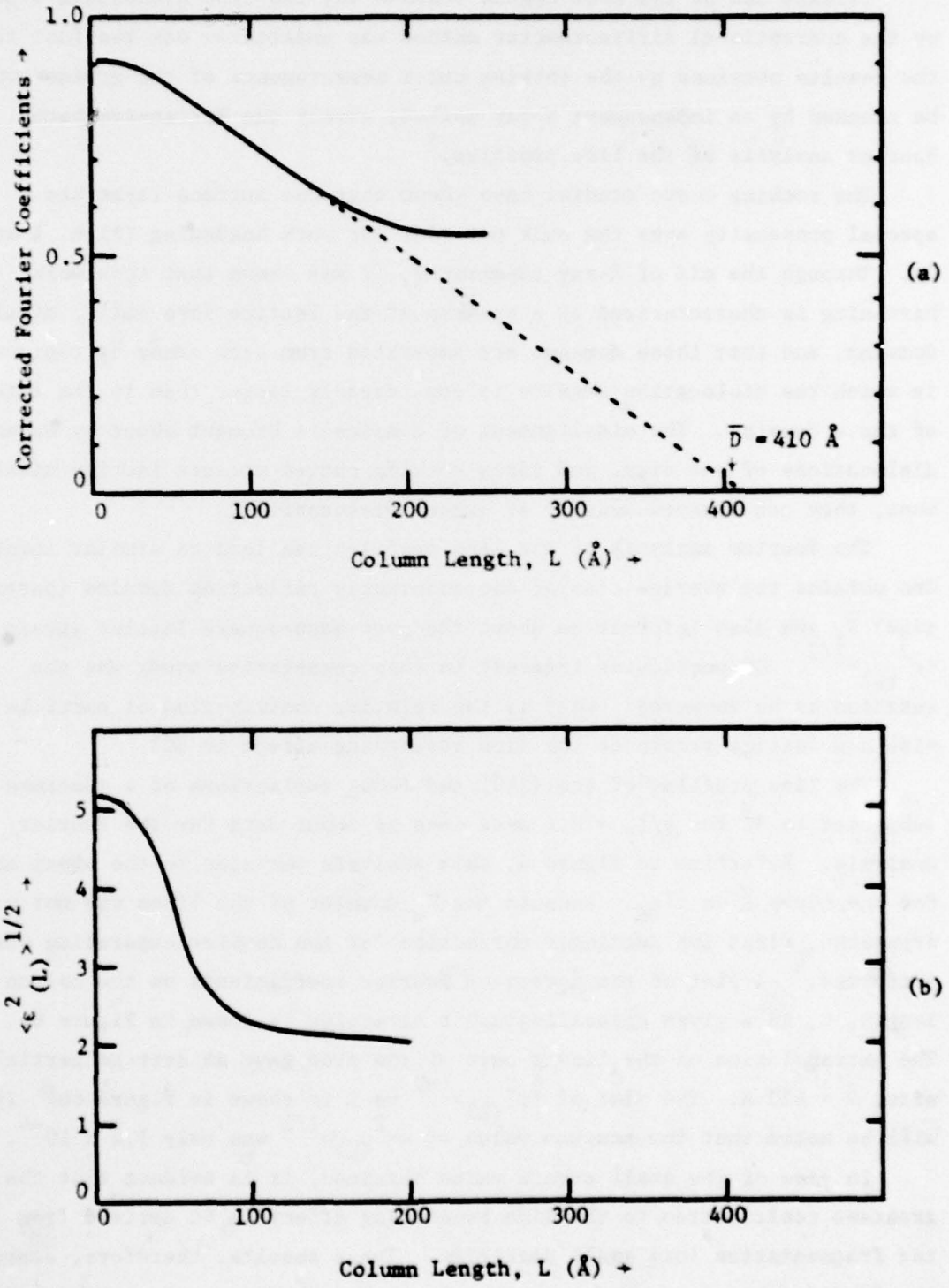


Figure 6. Results of Warren-Averbach Fourier analysis of the line profiles of SC. (a) Corrected Fourier coefficients vs the column length L. (b) Root-mean-square lattice strain $\langle \varepsilon^2_{(L)} \rangle^{1/2}$ vs the column length L.

utilized the values of $\bar{D}$ and $\langle\varepsilon^2_{(L)}\rangle^{1/2}$ to calculate dislocation densities. For the total dislocation density surrounding the particles, $\rho_D = 1/D^2$, one obtains the value $5.9 \times 10^{10}$ dislocations per $cm^2$. For the total dislocation density due to lattice strains, $\rho_S = 12\langle\varepsilon^2_{(L)}\rangle^{1/2}/b$, the value $5.4 \times 10^9$ dislocations per $cm^2$ was obtained. The latter value is smaller by one order of magnitude.

## Identification and Topography of Grains Analyzed for Their Defect Structure and SC Specificity

It has been shown previously[1] that because of the low stress applied in SC experiments, excessive grain rotation was avoided; consequently, due to the precise repositioning of the specimen, the identical grain reflections could be retained. Thus the lattice defects of the identical grains could be analyzed both as a function of fracture time, while exposed to conditions of SC, and of depth distance from the surface, for a given $t/t_c$.

Because of this unique feature which the X-ray double-crystal diffractometry offers, namely that those grains that exhibit pronounced susceptibility to SC can be analyzed selectively, considerable effort was expended to combine this method with X-ray reflection topography. The purpose of developing the capability of identifying and locating the sites of the analyzed grains on the specimen surface was to establish a link with other important methods of topographic grain analysis, namely optical metallography, TEM and SEM.

Figures 7a and 7b show the metallograph and X-ray reflection micrograph, respectively, of an annealed 304 stainless steel sample. The identity of a few grains is given by numbers. The individual reflection images can be traced outward in space by recording the images photographically at increasing distances from the specimen surface. By means of this tracing technique, there is established a direct correlation between the spot reflections on the Debye-Scherrer lines and the crystallites on the specimen surface giving rise to these reflections. Figures 8a and 8b show the spatial tracing of the grain reflections of 7b. Selected reflection micrographs at distances of 2.5 and 27.5 mm from the specimen surface are


(a)

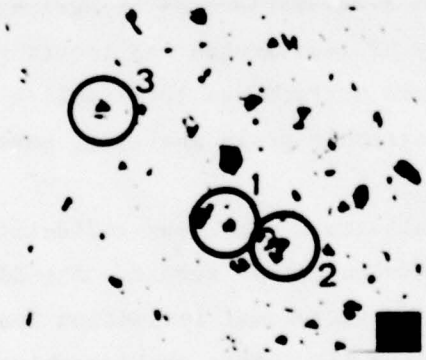


(b)

Figure 7. Identification of grains of 304 stainless steel. (a) Metallograph. (b) X-Ray reflection micrograph. Crystal-monochromated Cr $K_{\alpha}$ radiation.

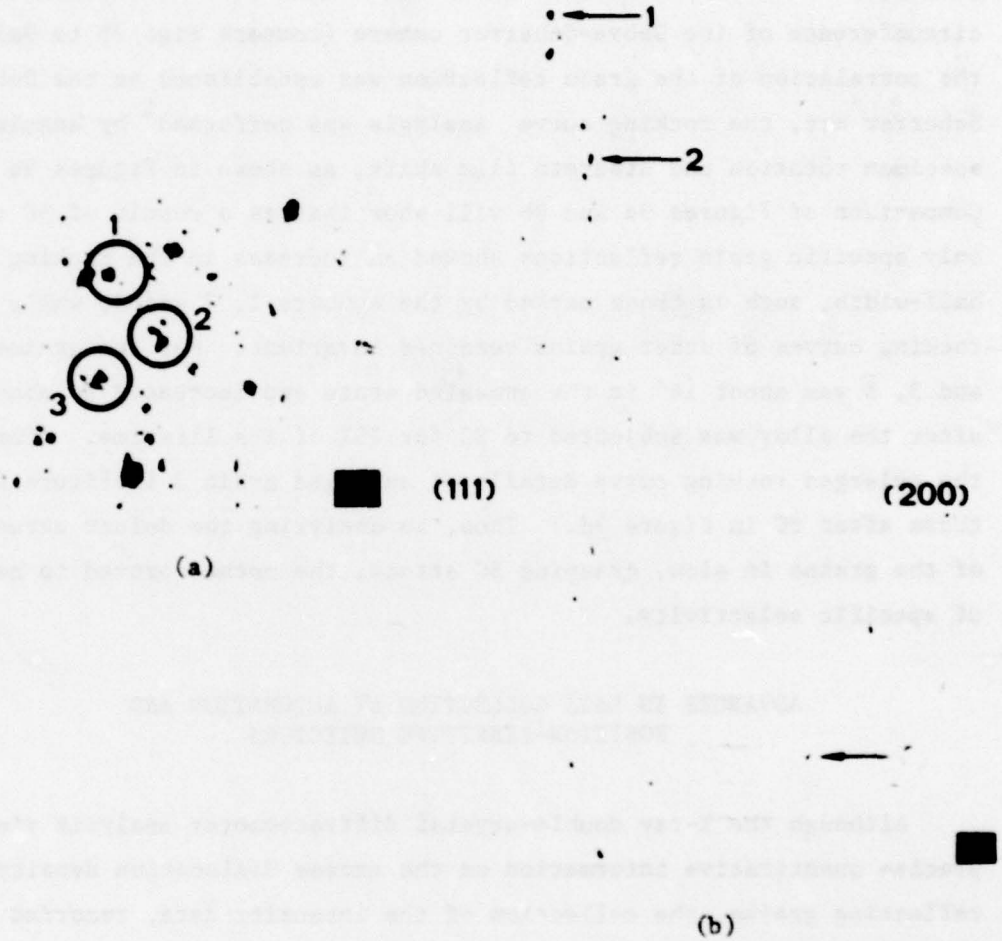


**Figure 8. Outward tracing of reflection images of Figure 7b. (a) 2.5 mm from specimen surface. (b) 27.5 mm from specimen surface.**

shown. For the sake of clarity, only three image reflections, marked by numbers 1, 2 and 3, are shown. It is perhaps worthwhile noting that, due to different crystal orientation, images that appeared in topographic proximity at the surface ended up at different (hkl) reflections on the circumference of the Debye-Scherrer camera (compare Fig. 7b to 9a). Once the correlation of the grain reflection was established at the Debye-Scherrer arc, the rocking curve analysis was performed[1] by angular specimen rotation and discrete film shift, as shown in Figures 9a and 9b. Comparison of Figures 9a and 9b will show that as a result of SC attack, only specific grain reflections showed an increase in the rocking curve half-width, such as those marked by the numbers 1, 2 and 3, while the rocking curves of other grains remained invariant. For the grains 1, 2 and 3, $\overline{\beta}$ was about 14' in the annealed state and increased to about 20' after the alloy was subjected to SC for 75% of its lifetime. (Compare the enlarged rocking curve details of annealed grain 3 in Figure 9c with those after SC in Figure 9d.) Thus, in analyzing the defect structure of the grains in slow, creeping SC attack, the method proved to be capable of specific selectivity.

## ADVANCES IN DATA COLLECTION BY AUTOMATION AND POSITION-SENSITIVE DETECTORS

Although the X-ray double-crystal diffractometer analysis yields precise quantitative information on the excess dislocation density of the reflecting grains, the collection of the intensity data, recorded on the photographic film as a function of specimen rotation, is admittedly somewhat time-consuming.[8] Typically each exposure of an array of spots, such as those shown in Figure 9, may take 30 minutes. An array of spots, representing the rocking curve of a grain, may consist of about 20 spots, so that the total time of exposure may extend to 10 hours. Subsequently, the recorded spot intensities are either visually estimated with the aid of a multiple-exposed film pack or, if a higher degree of precision is desired, they are analyzed by a microdensitometer. The latter operation is particularly time-consuming.

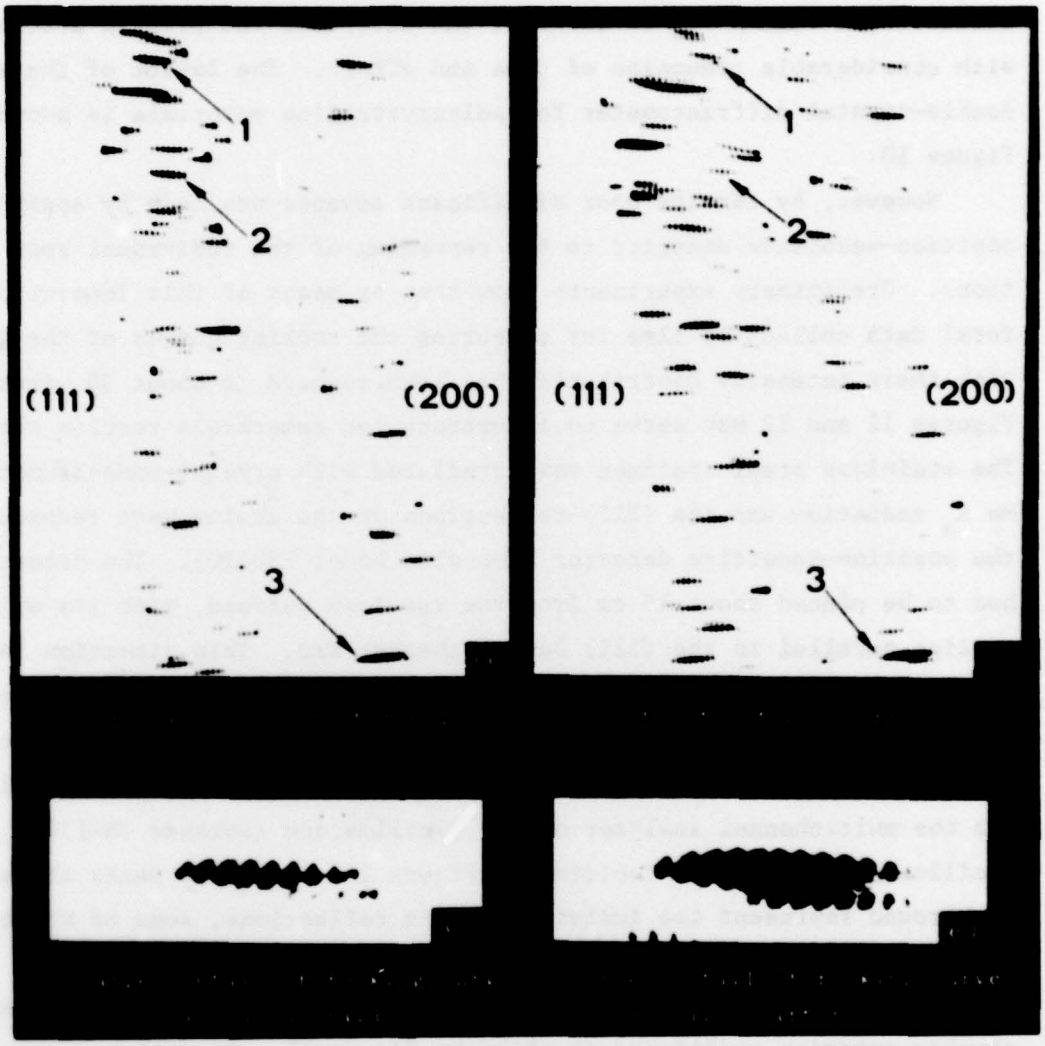


Figure 9. Detail of multiple-exposure diagram of 304 stainless steel. Array of spots represents samplings of the rocking curve of each reflecting grain. (Discrete, angular specimen rotation 3' of arc. Cr $K_{\alpha}$ radiation.)

Two significant advances in data collection have been made recently. One advance resulted from the automation of the X-ray double-crystal diffractometer. This development made it possible to program the specimen rotation and film shift as desired, and carry out the program automatically with considerable reduction of time and effort. The layout of the automated double-crystal diffractometer for polycrystalline materials is shown in Figure 10.

However, by far the most significant advance was made by applying a position-sensitive detector to the recording of the individual spot reflections. Preliminary experiments show that by means of this innovation, the total data collection time for measuring the rocking curves of the grains with their intensity distribution has been reduced to about 30 minutes. Figures 11 and 12 may serve to illustrate the remarkable results obtained. The stainless steel specimen was irradiated with crystal-monochromated Mo $K_\alpha$ radiation and the (111) reflections of the grains were recorded by the position-sensitive detector (Tennelec Model PSD110). The detector had to be placed about 15 cm from the specimen surface, with its wire section parallel to the (111) Debye-Scherrer arc. This direction is denoted in Figure 11 as the y-direction. The position of the beams reflected from the grains was analyzed by the electronic registering unit (Tennelec PSD1100), and the position and the intensity contribution were displayed via the multichannel analyzer on the oscilloscope (Norther TN-1705). The oscilloscope display is depicted in Figure 11, where the peaks above the background represent the individual grain reflections, some of which are denoted by letters.

The specimen was rotated in intervals of 3' of arc, and the discrete angular rotation positions are shown in Figure 11. It will be noted that the peak variations as a function of specimen rotation represent rocking curves of the grains. For example, grain D started its rocking curve at angular position 3', reached its peak at about position 12' and terminated the curve at position 21'. Thus the total reflecting range was about 18' of arc and the $\beta$ value was about 8' of arc. Figure 12 exhibits in greater detail the grain reflections corresponding to the angular rotation position 12', obtained by extending the exposure time by a few minutes.

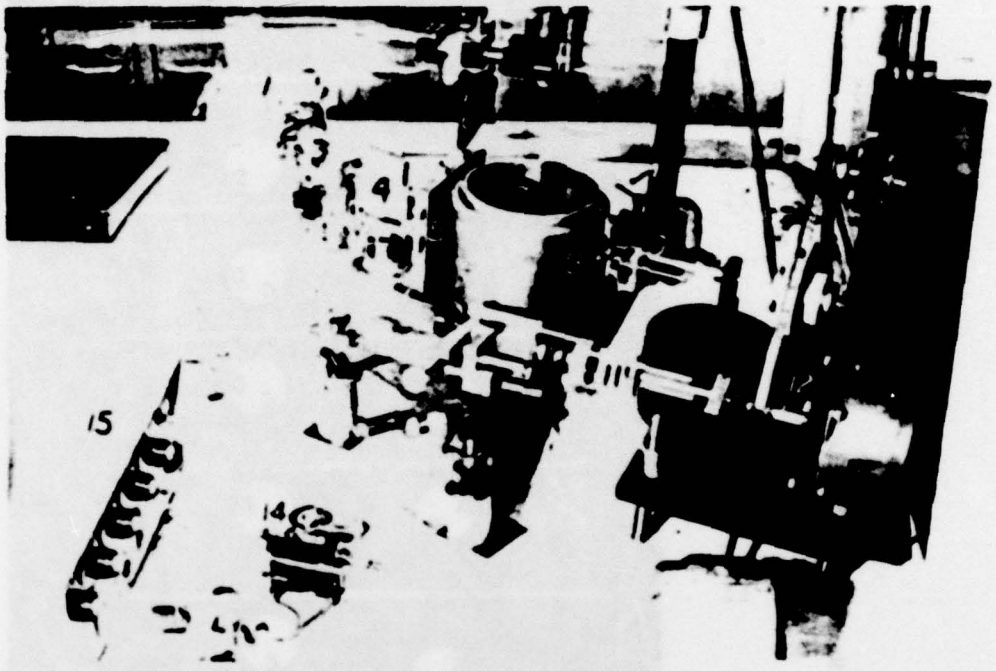


Figure 10. Automated double-crystal diffractometer.

1. X-Ray tube
2. Automatic shutter
3. Collimator
4. Monocrystal holder
5. Receiving slit
6. Berg-Barrett camera-film holder
7. Specimen holder and specimen
8. Debye-Scherrer camera-film holder
9. Film drive
10. Differential micrometer for specimen rotation
11. Micrometer drive
12. Power-transmitting gears
13. Stepping motor
14. Exposure-time controller
15. Stepping-motor controller

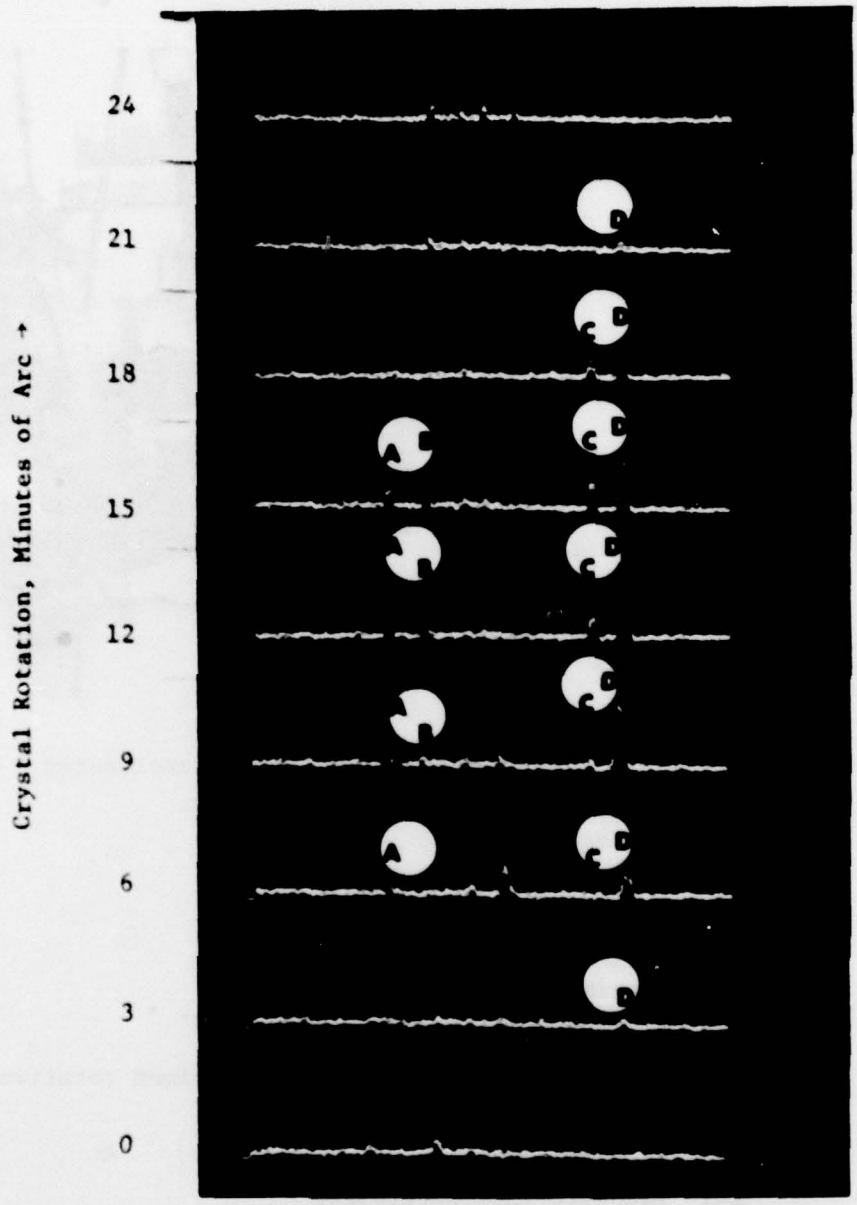


Figure 11. Rocking curve analysis of stainless steel grains by position-sensitive detector.

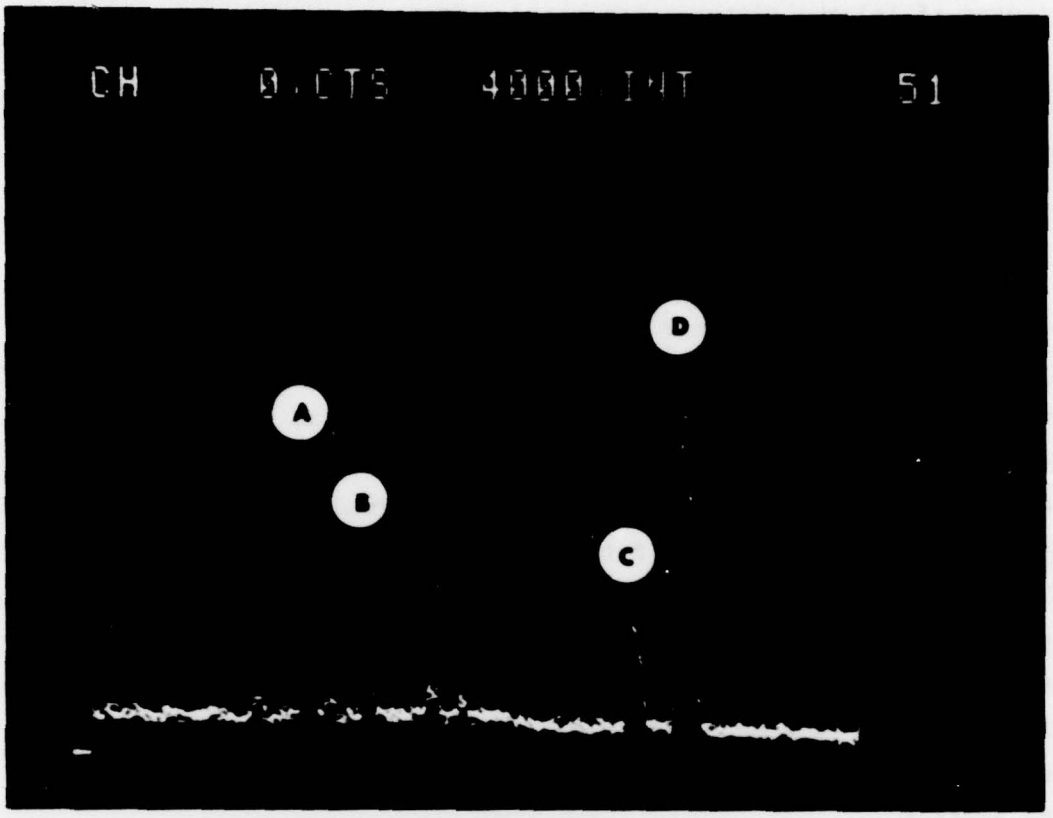


Figure 12. Detail of the grain reflections corresponding to the angular rotation position 12' in Figure 11.

It appears almost certain that the total time of collecting rocking curve data for a representative grain population can be reduced to a few minutes if (a) the distance between specimen and position-sensitive detector is shortened, which requires modification of the present experimental arrangement; (b) the registration of the data is interfaced with our PDP 1134 computer for storage and further analysis.

## CONCLUSIONS

The X-ray studies of 304 austenitic stainless steel subjected to stress corrosion (SC) and Al 2024-T4 subjected to corrosion fatigue (CF) have shown that the surface layer exhibits a special propensity for deformation when compared to the bulk of the material. An analogous behavior was found previously in tensile-deformed silicon, aluminum and gold single crystals and in fatigue-cycled aluminum single crystals and Al 2024-T3 alloy specimens.[3] The deformed surface layer is characterized by a decreasing gradient of excess dislocation density from the surface into the bulk. Whereas the gradient in the corrosion-fatigued aluminum alloy extended to a depth of 75-100 μm, the gradient in the SC of steel was much steeper, declining to its lowest value at about 10-25 μm from the surface.

As in the cycled Al alloys, the depth profile analysis of steel showed that the increase of excess dislocation density of the surface layer with corrosion time was also accompanied by an increase in the bulk. However, while the increase in the surface layer reached saturation rapidly, that in the bulk proceeded more gradually.

Whereas the penetration power of molybdenum radiation for aluminum alloys is such that it can probe the excess dislocation density in a depth region of 150-200 μm, which is well beyond the work-hardened surface layer, its penetration power is limited for steel. For steel subjected to SC, the depth penetration of molybdenum radiation extends only slightly beyond the deformed surface layer. Yet line broadening studies with this radiation showed that in the surface layer, saturation of the increase of excess dislocation density set in when the surface layer was no longer able to impede the egression of dislocations from the bulk (Fig. 4).

At this critical corrosion time, $t_{cr}$, cracks became visible (Fig. 5a). The saturation level of excess dislocation density in the surface layer is associated with a critical value of line broadening if conventional X-ray diffractometry is used, or with a critical rocking curve half-width $\overline{\beta}^*$ if the more precise double-crystal diffractometer method is applied. This value may be regarded as a parameter defining the limit of the integrity of the microstructure, for it was shown that with increased corrosion time this value remained invariant (Fig. 4) and that the remainder of the corrosion life from $t_{cr}$ onward was taken up with the development and propagation of a large failure crack (Fig. 5b).

The most important conclusion that emerged from this study appears to be the universal significance of $\overline{\beta}^*$, which seems to be the decisive parameter to assess the accrued damage in a structure, be it induced either by tensile deformation, fatigue, SC or CF. $\overline{\beta}^*$ can be obtained experimentally from careful measurements of the X-ray rocking curves of a representative grain population. This study has shown that the most promising and least time-consuming approach for efficient data collection is the use of position-sensitive detectors, which will register position and intensities of the grain reflections with great speed. The collected data are then sorted out, stored and analyzed via a multichannel analyzer and interface to a computer. If a lesser degree of accuracy in collecting data is acceptable, an alternative path can be taken by performing a Fourier analysis of the X-ray line profiles. The input data will then be based on conventional diffractometer measurements. For greater speed, position-sensitive detectors may be extremely helpful. Both experimental approaches are being investigated intensively.

## REFERENCES


1. Weissmann, S., Yazici, R., Tsakalakos, T., and Kramer, I. R., Interim Report ONR-R-1, December 1978.

2. Pangborn, R. N., Weissmann, S., and Kramer, I. R., Scripta Met., 12, 129 (1978).

3. Pangborn, R. N., Weissmann, S., and Kramer, I. R., Fatigue Eng. Mat., 1, 363-369 (1979).

4. Weissmann, S., Pangborn, R. N., and Kramer, I. R., in Fatigue Mechanisms, ASTM STP675, 1979, pp. 163-167.

5. Warren, B. E., and Averbach, B. L., J. Appl. Phys., 21, 595 (1950); 23, 497 (1952).

6. Rachinger, W. A., J. Sci. Inst., 25, 254 (1948).

7. Cohen, J. B., Diffraction Methods in Materials Science, Macmillan Company, New York, 1966, p. 315.

8. Weissmann, S., J. Appl. Phys., 27, 389 (1956).

# BASIC DISTRIBUTION LIST

Technical and Summary Reports April 1978

| Organization | Copies |
|---|---|
| Defense Documentation Center<br>Cameron Station<br>Alexandria, VA 22314 | 12 |
| Office of Naval Research<br>Department of the Navy<br>800 N. Quincy Street<br>Arlington, VA 22217 | |
| ATTN: Code 471 | 1 |
| Code 102 | 1 |
| Code 470 | 1 |
| Commanding Officer<br>Office of Naval Research<br>Branch Office<br>Building 114, Section D<br>666 Summer Street<br>Boston, MA 02210 | 1 |
| Commanding Officer<br>Office of Naval Research<br>Branch Office<br>536 South Clark Street<br>Chicago, IL 60605 | 1 |
| Office of Naval Research<br>San Francisco Area Office<br>One Hallidie Plaza Suite 601<br>San Francisco, CA 94102 | 1 |
| Naval Research Laboratory<br>Washington, DC 20375 | |
| ATTN: Codes 6000 | 1 |
| 6100 | 1 |
| 6300 | 1 |
| 6400 | 1 |
| 2627 | 1 |
| Naval Air Development Center<br>Code 302<br>Warminster, PA 18964<br>ATTN: Mr. F. S. Williams | 1 |

| Organization | Copies |
|---|---|
| Naval Air Propulsion Test Center<br>Trenton, NJ 08628<br>ATTN: Library | 1 |
| Naval Construction Batallion<br>Civil Engineering Laboratory<br>Port Hueneme, CA 93043<br>ATTN: Materials Division | 1 |
| Naval Electronics Laboratory<br>San Diego, CA 92152<br>ATTN: Electron Materials<br>Sciences Division | 1 |
| Naval Missile Center<br>Materials Consultant<br>Code 3312-1<br>Point Mugu, CA 92041 | 1 |
| Commanding Officer<br>Naval Surface Weapons Center<br>White Oak Laboratory<br>Silver Spring, MD 20910<br>ATTN: Library | 1 |
| David W. Taylor Naval Ship<br>Research and Development Center<br>Materials Department<br>Annapolis, MD 21402 | 1 |
| Naval Undersea Center<br>San Diego, CA 92132<br>ATTN: Library | 1 |
| Naval Underwater System Center<br>Newport, RI 02840<br>ATTN: Library | 1 |
| Naval Weapons Center<br>China Lake, CA 93555<br>ATTN: Library | 1 |
| Naval Postgraduate School<br>Monterey, CA 93940<br>ATTN: Mechanical Engineering<br>Department | 1 |

BASIC DISTRIBUTION LIST (cont'd)

| Organization | Copies |
|---|---|
| Naval Air Systems Command<br>Washington, DC 20360<br>ATTN: Codes 52031<br>52032 | 1 |
| Naval Sea System Command<br>Washington, DC 20362<br>ATTN: Code 035 | 1 |
| Naval Facilities Engineering Command<br>Alexandria, VA 22331<br>ATTN: Code 03 | 1 |
| Scientific Advisor<br>Commandant of the Marine Corps<br>Washington, DC 20380<br>ATTN: Code AX | 1 |
| Naval Ship Engineering Center<br>Department of the Navy<br>Washington, DC 20360<br>ATTN: Code 6101 | 1 |
| Army Research Office<br>P.O. Box 12211<br>Triangle Park, NC 27709<br>ATTN: Metallurgy & Ceramics Program | 1 |
| Army Materials and Mechanics Research Center<br>Watertown, MA 02172<br>ATTN: Research Programs Office | 1 |
| Air Force Office of Scientific Research<br>Bldg. 410<br>Bolling Air Force Base<br>Washington, DC 20332<br>ATTN: Chemical Science Directorate<br>Electronics & Solid State Sciences Directorate | 1<br>1 |
| Air Force Materials Laboratory<br>Wright-Patterson AFB<br>Dayton, OH 45433 | 1 |
| Library<br>Building 50, Rm 134<br>Lawrence Radiation Laboratory<br>Berkeley, CA | 1 |

| Organization | Copies |
|---|---|
| NASA Headquarters<br>Washington, DC 20546<br>ATTN: Code RRM | 1 |
| NASA<br>Lewis Research Center<br>21000 Brookpark Road<br>Cleveland, OH 44135<br>ATTN: Library | 1 |
| National Bureau of Standards<br>Washington, DC 20234<br>ATTN: Metallurgy Division<br>Inorganic Materials Div. | 1<br>1 |
| Director Applied Physics Laboratory<br>University of Washington<br>1013 Northeast Forthieth Street<br>Seattle, WA 98105 | 1 |
| Defense Metals and Ceramics Information Center<br>Battelle Memorial Institute<br>505 King Avenue<br>Columbus, OH 43201 | 1 |
| Metals and Ceramics Division<br>Oak Ridge National Laboratory<br>P.O. Box X<br>Oak Ridge, TN 37380 | 1 |
| Los Alamos Scientific Laboratory<br>P.O. Box 1663<br>Los Alamos, NM 87544<br>ATTN: Report Librarian | 1 |
| Argonne National Laboratory<br>Metallurgy Division<br>P.O. Box 229<br>Lemont, IL 60439 | 1 |
| Brookhaven National Laboratory<br>Technical Information Division<br>Upton, Long Island<br>New York 11973<br>ATTN: Research Library | 1 |
| Office of Naval Research<br>Branch Office<br>1030 East Green Street<br>Pasadena, CA 91106 | 1 |

| Organization | Copies |
|---|---|
| Naval Air Systems Command<br>Washington, DC 20360<br>ATTN: Codes 52031<br>52032 | 1 |
| Naval Sea System Command<br>Washington, DC 20362<br>ATTN: Code 035 | 1 |
| Naval Facilities Engineering Command<br>Alexandria, VA 22331<br>ATTN: Code 03 | 1 |
| Scientific Advisor<br>Commandant of the Marine Corps<br>Washington, DC 20380<br>ATTN: Code AX | 1 |
| Naval Ship Engineering Center<br>Department of the Navy<br>Washington, DC 20360<br>ATTN: Code 6101 | 1 |
| Army Research Office<br>P.O. Box 12211<br>Triangle Park, NC 27709<br>ATTN: Metallurgy & Ceramics Program | 1 |
| Army Materials and Mechanics Research Center<br>Watertown, MA 02172<br>ATTN: Research Programs Office | 1 |
| Air Force Office of Scientific Research<br>Bldg. 410<br>Bolling Air Force Base<br>Washington, DC 20332<br>ATTN: Chemical Science Directorate<br>Electronics & Solid State Sciences Directorate | 1<br>1 |
| Air Force Materials Laboratory<br>Wright-Patterson AFB<br>Dayton, OH 45433 | 1 |
| Library<br>Building 50, Rm 134<br>Lawrence Radiation Laboratory<br>Berkeley, CA | 1 |

| Organization | Copies |
|---|---|
| NASA Headquarters<br>Washington, DC 20546<br>ATTN: Code RRM | 1 |
| NASA<br>Lewis Research Center<br>21000 Brookpark Road<br>Cleveland, OH 44135<br>ATTN: Library | 1 |
| National Bureau of Standards<br>Washington, DC 20234<br>ATTN: Metallurgy Division<br>Inorganic Materials Div. | 1<br>1 |
| Director Applied Physics Laboratory<br>University of Washington<br>1013 Northeast Forthieth Street<br>Seattle, WA 98105 | 1 |
| Defense Metals and Ceramics Information Center<br>Battelle Memorial Institute<br>505 King Avenue<br>Columbus, OH 43201 | 1 |
| Metals and Ceramics Division<br>Oak Ridge National Laboratory<br>P.O. Box X<br>Oak Ridge, TN 37380 | 1 |
| Los Alamos Scientific Laboratory<br>P.O. Box 1663<br>Los Alamos, NM 87544<br>ATTN: Report Librarian | 1 |
| Argonne National Laboratory<br>Metallurgy Division<br>P.O. Box 229<br>Lemont, IL 60439 | 1 |
| Brookhaven National Laboratory<br>Technical Information Division<br>Upton, Long Island<br>New York 11973<br>ATTN: Research Library | 1 |
| Office of Naval Research<br>Branch Office<br>1030 East Green Street<br>Pasadena, CA 91106 | 1 |

C
April 1978

SUPPLEMENTARY DISTRIBUTION LIST

Technical and Summary Reports

Dr. T. R. Beck
Electrochemical Technology Corporation
10035 31st Avenue, NE
Seattle, Washington 98125

Professor I. M. Bernstein
Carnegie-Mellon University
Schenley Park
Pittsburgh, Pennsylvania 15213

Professor H. K. Birnbaum
University of Illinois
Department of Metallurgy
Urbana, Illinois 61801

Dr. Otto Buck
Rockwell International
1049 Camino Dos Rios
P. O. Box 1085
Thousand Oaks, California 91360

Dr. David L. Davidson
Southwest Research Institute
8500 Culebra Road
P. O. Drawer 28510
San Antonio, Texas 78284

Dr. D. J. Duquette
Department of Metallurgical Engineering
Rensselaer Polytechnic Institute
Troy, New York 12181

Professor R. T. Foley
The American University
Department of Chemistry
Washington, D. C. 20016

Mr. G. A. Gehring
Ocean City Research Corporation
Tennessee Avenue & Beach Thorofare
Ocean City, New Jersey 08226

Dr. J. A. S. Green
Martin Marietta Corporation
1450 South Rolling Road
Baltimore, Maryland 21227

Professor R. H. Heidersbach
University of Rhode Island
Department of Ocean Engineering
Kingston, Rhode Island 02881

Professor H. Herman
State University of New York
Material Sciences Division
Stony Brook, New York 11794

Professor J. P. Hirth
Ohio State University
Metallurgical Engineering
Columbus, Ohio 43210

Dr. E. W. Johnson
Westinghouse Electric Corporation
Research and Development Center
1310 Beulah Road
Pittsburgh, Pennsylvania 15235

Professor R. M. Latanision
Massachusetts Institute of Technology
77 Massachusetts Avenue
Room 8-202
Cambridge, Massachusetts 02139

Dr. F. Mansfeld
Rockwell International Science Center
1049 Camino Dos Rios
P. O. Box 1085
Thousand Oaks, California 91360

Professor H. W. Pickering
Pennsylvania State University
Department of Material Sciences
University Park, Pennsylvania 16802

Dr. E. A. Starke, Jr.
Georgia Institute of Technology
School of Chemical Engineering
Atlanta, Georgia 30332

Dr. Barry C. Syrett
Stanford Research Institute
333 Ravenswood Avenue
Menlo Park, California 94025

C
April 1978

SUPPLEMENTARY DISTRIBUTION LIST
(Continued)

Dr. R. P. Wei
Lehigh University
Institute for Fracture and
Solid Mechanics
Bethlehem, Pennsylvania 18015

Professor H. G. F. Wilsdorf
University of Virginia
Department of Materials Science
Charlottesville, Virginia 22903

Prof. J. B. Cohen
Dept. of Materials Science & Engineering
The Technological Institute
Northwestern University
Evanston, Illinois 60201

Prof. H. W. Liu
Dept. of Chemical Engineering & Materials Science
L. C. Smith College of Engineering
Syracuse University
Syracuse, NY 13210

Dr. S. P. Rideout
Savannah River Laboratory
E. I. duPont de Nemours & Co
Aiken, South Carolina 29801

Prof. R. W. Staehle
Dept. of Metallurgical Engineering
The Ohio State University
Columbus, Ohio 43210